Adaptive Optics Imaging in Patients Affected by Pseudoxanthoma Elasticum

VITTORIA MURRO, DARIO PASQUALE MUCCIOLO, DARIO GIORGIO, LAURA PAVESE, FEDERICA BORALDI, DANIELA QUAGLINO, LUCIA FINOCCHIO, ANDREA SODI, GIANNI VIRGILI, AND FABRIZIO GIANSANTI

• PURPOSE: To describe the retinal findings of patients affected by pseudoxanthoma elasticum (PXE) using a multimodal imaging approach including flood-illumination adaptive optics ophthalmoscopy (AO).

• DESIGN: Retrospective case series.

• MATERIALS AND METHODS: Patients affected by PXE were retrospectively studied. Clinical data, color, infrared and autofluorescence fundus imaging, optical coherence tomographic scans, and AO examinations were collected. Furthermore, the photoreceptor count was assessed. PXE diagnosis was confirmed by a positive skin biopsy and/or genetic testing.

• RESULTS: Twenty-one eyes of 18 patients (11 females and 7 males) were included in the study. In 3 patients, both eyes were studied. The mean age at examination was 37.7 ± 16.4 years (range 14-66) and the mean best-corrected visual acuity (BCVA) was 0.1 ± 0.2 logMAR (range 0-1). We identified 3 types of angioid streaks (AS) using AO: "crack," "band," and "hypopigmented." The first 2 were very similar and they differed in size; the third type showed specific clinical features. Comet lesions appeared as hyper-reflective round lesions on AO imaging. In all eyes, the cone mosaic appeared reduced inside the streaks compared to the neighboring areas (13,532.8 ± 1,366.5 cones/mm^2 vs 16,817.1 ± 1,263.0 cones/mm^2 respectively).

• CONCLUSION: Using AO imaging in PXE-related retinopathy, we were able to observe the presence of the photoreceptors within the angioid streaks, differentiate 3 types of angioid streaks, based on size and reflective features, and identify the very small crystalline bodies not identifiable using other retinal imaging techniques. (Am J Ophthalmol 2021;224:84–95. © 2020 Elsevier Inc. All rights reserved.)

Accepted for publication Dec 4, 2020.

From the Department of Neuroscience, Psychology, Drug Research and Child Health, University of Florence (V.M., D.P.M., D.G., L.P., F.B., L.F., A.S., G.V., F.G.), Florence, Italy; and Department of Life Sciences, University of Modena and Reggio Emilia (F.B., D.Q.), Modena, Italy

Inquiries to Dario Pasquale Mucciolo, Department of Neuroscience, Psychology, Drug Research and Child Health, University of Florence, Careggi Teaching Hospital, Largo Brambilla, 3-50134 Florence, Italy; e-mail: dario.mucciolo@gmail.com

PSEUDOXANTHOMA ELASTICUM (PXE; OMIM 264800) IS an inherited multisystem disease affecting mainly the skin, the cardiovascular system, and the eyes, with an estimated prevalence of 1:25,000 to 50,000.[1] PXE is caused by mutations in the *ABCC6* gene on chromosome 16p13.1, although mutations in other genes leading to a progressive calcification of elastic fibers in soft connective tissues such as dermis, blood vessels, and Bruch membrane have already been described.[2–5] Typical ocular findings classically include peau d'orange, angioid streaks, comet lesions, and optic nerve drusen.[6–9] Further investigations have suggested that peau d' orange represents subconfluent calcification of Bruch membrane, whereas the more confluent calcified regions, called the "coquille d'oeuf" or eggshell, are the more brittle Bruch membrane areas, and therefore subject to fracture.[10] Additional findings, usually appearing late during the course of the disease, are pattern dystrophy-like changes,[11] choroidal neovascularization,[12] and areas of chorioretinal atrophy that can spread even into the midperiphery of the retina.[13,14] Flood-illumination adaptive optics (AO) ophthalmoscopy is a novel imaging tool that provides high-resolution images of retinal microstructures, including photoreceptors, capillaries, and nerve fiber bundles.[15] Conventional imaging has been widely used to characterize PXE-related retinopathy findings although little is known about the use of AO features in the imaging of eyes of PXE patients.[16,17] In this study, we have described retinal features of patients affected by PXE-related retinopathy using a multimodal imaging approach and AO examinations.

MATERIALS AND METHODS

THE STUDY WAS APPROVED BY THE LOCAL ETHICS COMMITtee and adhered to the Declaration of Helsinki. Patients affected by PXE (identified using a computer database search) were retrospectively evaluated at the Regional Reference Center for Hereditary Retinal Degenerations at the Careggi Teaching Hospital in Florence, Italy. The diagnosis of PXE was positively confirmed by PXE fundus findings (including peau d'orange, angioid streaks, and comet lesions), genetic testing results, and skin biopsy.

Patients included in our study received a comprehensive ophthalmologic examination including best-corrected visual acuity (BCVA) measurement (logMAR unit),

0002-9394/$36.00
https://doi.org/10.1016/j.ajo.2020.12.007

intraocular pressure evaluation, biomicroscopy of the anterior segment, and funduscopy. Color fundus photographs (FF450 Retinograph; Carl Zeiss Meditec, Jena, Germany), optical coherence tomography (OCT) (Swept Source OCT instrument DRI OCT-1 [Topcon, Tokyo, Japan] and Spectralis HRA-OCT [Heidelberg Engineering, Heidelberg, Germany]), fundus autofluorescence (FAF) (ultrawide-field FAF imaging; Daytona [Optos, Optos plc, Dunfermline, UK] and Spectralis HRA OCT [Heidelberg Engineering]) were performed. More specifically, infrared reflectance imaging (IR) was obtained using ultrawidefield digital scanning laser technology (Daytona; Optos) and/or Spectralis HRA OCT (Heidelberg Engineering).

• **GENETIC EXAMINATION:** Rare sequence variants in *ABCC6* gene were detected by Sanger sequencing on genomic DNA isolated from whole blood (QIAamp blood kit; Qiagen GmbH, Hilden, Germany) as previously described.[18] For rare sequence variants not yet reported in literature, classified as pathogenic, the pathogenicity score was predicted by in silico analyses[5] using Sorting Intolerant From Tolerant (SIFT), Polymorphism Phenotyping (Polyphen2), Panther.

• **AO IMAGING:** All patients were imaged using a flood-illuminated AO retinal camera (rtx1 AO retinal camera; Imagine Eyes, Orsay, France). A full description of the rtx1 has previously been published.[19] To better characterize specific AO-PXE-related retinopathy findings, all the images of eyes with good visual acuity and good fixation were selected. An 850-nm LED was used to illuminate the fundus of the eye and a low-noise CCD camera was used to capture the raw images of the retina at 10 Hz over a 4-degree × 4-degree field of view. Duration of the examination was approximately 15 minutes per patient. Sets of 40 short exposure time images were recorded to obtain one improved (composite) final image of the fundus; thus, AO images of the macula and of the peripapillary regions were acquired for each eye. Furthermore, the final image (montage image) was obtained by combining multiple single images using the I2K retina software (Dual Align). Refractive error and axial length were used for assessing cone photoreceptor counts in all eyes. Cone density was analyzed in a region of interest (ROI) within the angioid streaks and in the neighboring areas, and expressed as mean ± SD. This was carried out using a custom software package AO Detect Mosaic V.0.1 (Imagine Eyes). The manufacturer's software automatically detects the cone mosaic and the position of the photoreceptors, and this allows us to quantitatively evaluate the photoreceptors. The software detects "bright" hyper-reflective small circular spots with different reflectivity from the surrounding background; the spatial distribution of the centers of these spots was analyzed in terms of local cell numerical density (number of cones per square millimeter of retinal surface; cones/mm^2).[20] In this study, the patients were assigned an anonymous ID.

RESULTS

TWENTY-ONE EYES OF 18 PATIENTS WERE EXAMINED IN THE study (in 3 patients, we studied both eyes). At examination, the mean (±SD) age of patients was 37.7 ± 16.4 years (range 14-66). The mean (±SD) best-corrected visual acuity (BCVA) was 0.1 ± 0.2 logMAR (range 1-0). All eyes were phakic. The mean spherical equivalent was –1.1 ± 2.8. A positive skin biopsy was available for 8 patients (8/18; 44.4%) and genetic examination was performed on 16 patients (16/18; 88.9%). In particular, molecular analysis revealed the presence of 20 distinct rare sequence variants in our cohort, of which 4 had not previously been reported (c.1145G>A, c.1961C>T, c.2095G>A, and c.3989T>C). Most were missense mutations (11 of 20, 55%), but there was also 1 deletion and 1 insertion, 2 splicing, and 5 nonsense mutations. Nine of 16 patients (9/16) were compound heterozygous for pathogenic sequence variants in the *ABCC6* gene. Five patients (5/16) were carriers of a pathogenic variant in the homozygous state. Two patients (2/16, P3 and P13) were characterized by a single mutation in the *ABCC6* gene and were included in the study because they presented eye findings and a positive skin biopsy compatible with PXE. Genetic examination was not available for 2 patients (P8 and P12) but they were included because they had a positive skin biopsy (compatible with PXE diagnosis). Patients P6 and P7 were twin sisters.

Clinical and molecular findings have been summarized in Table 1.

• **FUNDUS IMAGING FINDINGS:** Angioid streaks (AS) were detectable in 20 eyes (20/21; 95.2%) of 17 patients and appeared as reddish-brown or grayish fissures of variable size on color fundus photographs, as dark fissures (hyporeflective) against a lighter background on IR, and as hypo-autofluorescent abnormalities (more or less continuous) on FAF imaging (Figures 1 and 2). In 3 eyes of 2 patients, angioid streaks appeared as small hypopigmented lines on color fundus photographs, with hyper-reflective features on IR imaging, and as hypo-autofluorescent changes on FAF imaging (Figure 3). Some AS were concentric to the optic disc, whereas others had a radiating pattern extending from the optic nerve head to the midperiphery. More specifically, in 8 eyes of 7 patients, the AS were confined only to the peripapillary area whereas in the remaining eyes the AS involved the posterior pole and the midperiphery.

At the OCT examination, undulations of the Bruch membrane with very mild to severe irregularities of the interdigitation zone (IZ) and retinal pigment epithelium could be detected overlying the AS in all eyes in our series. The "cracked eggshell" condition was identified in 1 eye of 1 patient (left eye of patient P10): this clinical finding was characterized by the presence of several dark, irregular,

TABLE 1. Clinical and Molecular Findings

Patient ID	Sex	Age	Eye	BCVA	Spherical Equivalent	Angioid Streaks (AO Type)	Multimodal Imaging Classification	cDNA	Protein	Reference
1	F	61	OS	0.0	2.0	1	Crack	c.1145G>A c.3989T>C	p.Arg382Gln p.Ile1330Thr	Present study
2	M	66	OD	0.0	–2.5	2	Band	c.3421C>T c.4198G>A	p.Arg1141* p.Glu1400Lys	Götting et al, 2004[21]; Chassaing et al, 2004[22]
3	F	26	OD	0.0	0	1	Crack	Exon24_27del	Deletion	Costropt et al, 2010[23]
4	F	28	OS	0.0	–6	1.2	Crack and band	c.1132C>T c.3421C>T	p.Gln378* p.Arg1141*	Pulkkinen et al, 2001[24]; Götting et al, 2004[21]
5	F	58	OS	0.1	0	2	Band	c.3421C>T c.3421C>T	p.Arg1141* p.Arg1141*	Götting et al, 2004[21]
6	F	22	OS	0.0	–4.5	3	Hypopigmented	c.2247+1G>A c.3661C>T	splicing p.Arg1221Cys	Boraldi et al, 2014[25]; Noji et al, 2004[26]
7	F	22	OD	0.0	–8.25	2.3	Band and hypopigmented	c.2247+1G>A c.3661C>T	splicing p.Arg1221Cys	Boraldi et al, 2014[25]; Noji et al, 2004[26]
8	M	48	OS	0.1	–0.75	2	Band	not available		
9	F	38	OD	0.0	–4	2	Band	c.1857dupC c.2294G>A	p.Ser620Leufs*121 p.Arg765Gln	Pfendner et al, 2007[27]; Le Saux 2001[28]
	F	38	OS	0.0	–4.25	2	Band			
10	M	24	OD	0.0	0	1.2	Crack and band	c.3413G>A	p.Arg1138Gln	Ringpfeil et al, 2000[29]
	M	24	OS	0.0	0	1.2	Crack and band	c.3413G>A	p.Arg1138Gln	
11	M	15	OD	0.0	0	3	Hypopigmented	c.1961C>T c.2095G>A c.3490C>T	p.Pro654Leu p.Glu699Lys p.Arg1164*	Present study; Present study; Struk et al, 2000[3]
12	F	58	OD	1.0	1.75	2	Band	not available		
13	M	14		0.0	3	0	No angioid streaks	c.1132C>T	p.Gln378*	Pulkkinen et al, 2001[24]
14	M	40	OD	0.0	0	1	Crack	c.3340C>T c.3340C>T	p.Arg1114Cys p.Arg1114Cys	Gheduzzi et al, 2004[30]
15	F	52	OD	0.2	–0.75	2	Band	c.2018T>C, c.2787+1G>T	p.Leu673Pro splicing	Le Saux, 2001[28]; Le Saux et al, 2000[2]
16	M	43	OD	0.0	0.75	2	Band	c.1553G>A	p.Arg518Gln	Uitto et al, 2001[31]
	M	43	OS	0.0	0.75			c.1553G>A	p.Arg518Gln	
17	F	38	OS	0.0	–1.25	1	Crack	c.1552C>T c.3421C>T	p.Arg518* p.Arg1141*	Meloni et al, 2001[32]; Götting et al, 2004[21]
18	F	27	OS	0.0	0	1	Crack	c.1308G>A c.1308G>A	p.Trp436* p.Trp436*	Guerra et al, 2009[33]

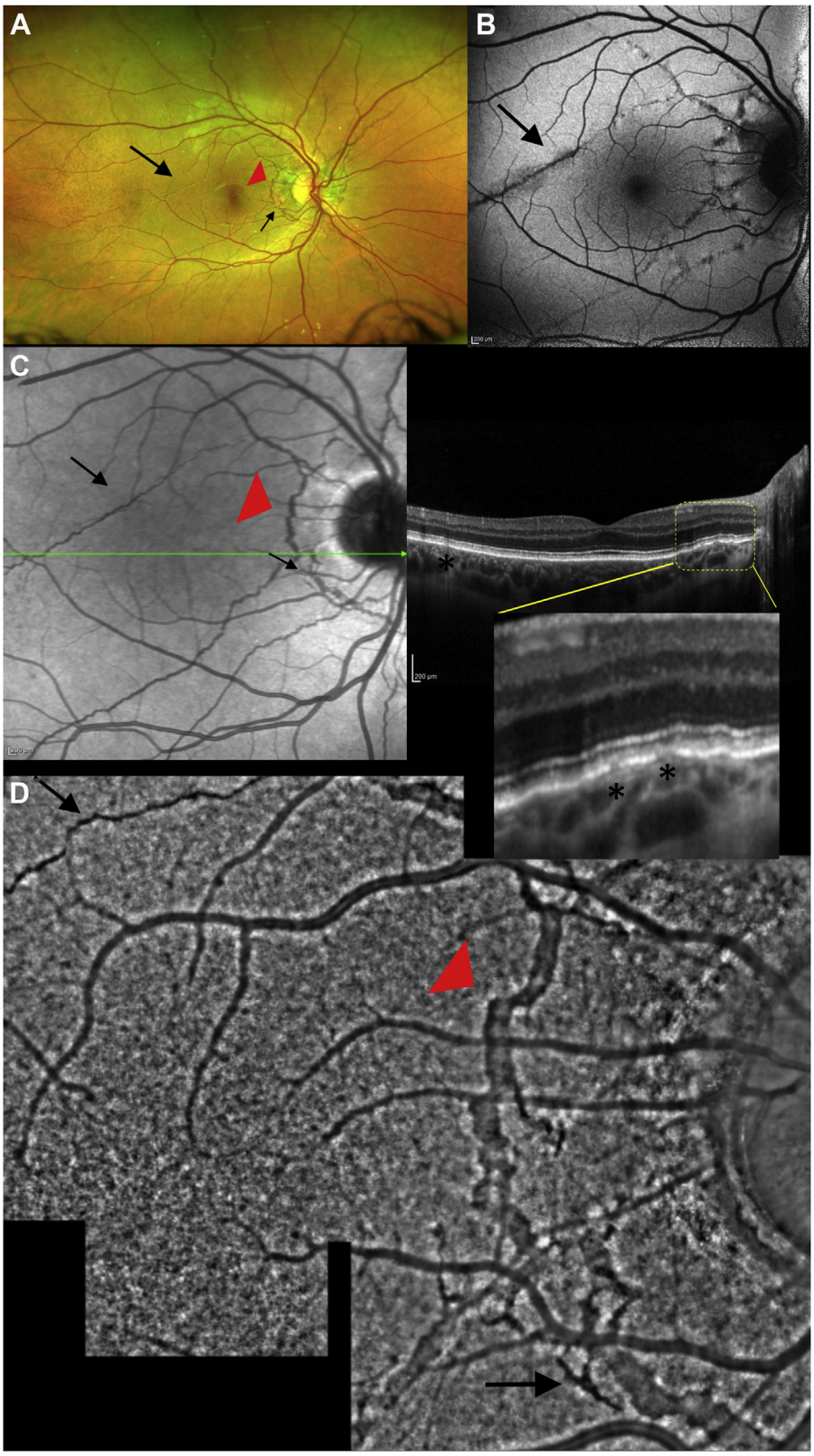

FIGURE 1. (A) CFP, (B) FAF, (C) IR imaging with OCT B-scan, and (D) AO showing angioid streaks of Type 1 (crack type) and Type 2 (band type). Black arrows indicate crack type whereas red arrowheads indicate band type. OCT examination (C, right part) shows the retinal pigment epithelium–Bruch membrane interruptions (black asterisks) corresponding to the angioid streaks showed as hyporeflective streaks on IR (C, left part) particularly evident in the magnified image. AO = adaptive optics, CFP = color fundus photograph, FAF = fundus autofluorescence, IR = infrared imaging, OCT = optical coherence tomography.

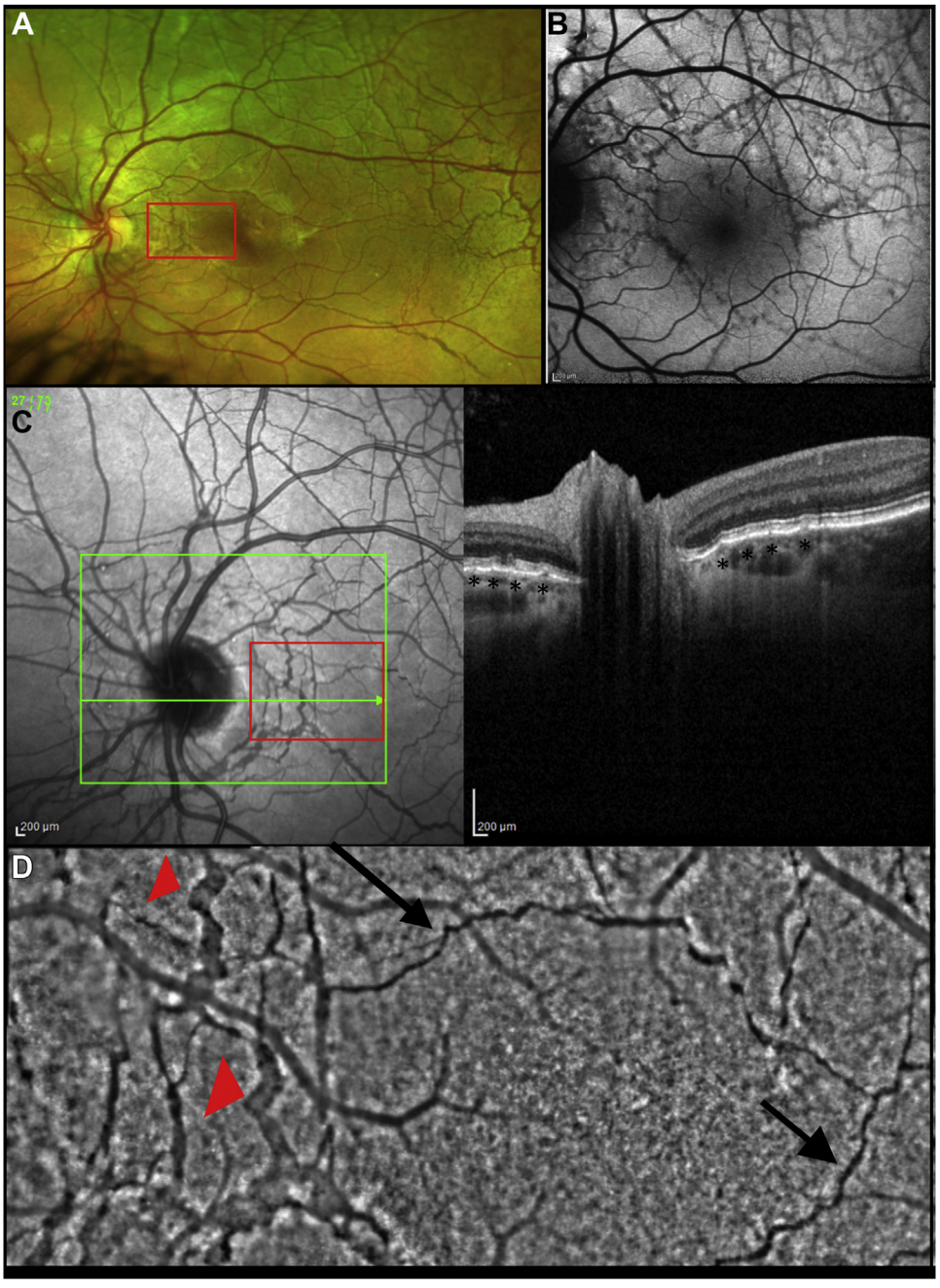

FIGURE 2. (A) CFP and (B) FAF showing multiple angioid streaks; the red rectangle in (A) CFP and in (C) IR imaging showing the AO image location. The "cracked eggshell" is evident because of the presence of several dark, irregular, linear fractures detectable as hyporeflective lesions on (C) IR imaging and hypo-autofluorescent abnormalities on (B) FAF imaging. (C) OCT examination shows the multiple retinal pigment epithelium–Bruch membrane interruptions (asterisks). (D) AO imaging reveals crack (black arrows) and band type (red arrowheads) of angioid streaks. AO = adaptive optics, CFP = color fundus photograph, FAF = fundus autofluorescence, IR = infrared, OCT = optical coherence tomography.

linear fractures detectable as hyporeflective lesions on IR imaging and hypo-autofluorescent abnormalities on FAF imaging.

Peau d'orange was visible in all eyes of our series and appeared as yellowish nonconfluent dot-like lesions scattered from the posterior pole to the midperipheral retina and were prominently visible in the temporal region. These alterations were better highlighted at color and IR imaging, whereas they were not detectable at the FAF examination in any eyes of our series. Optic nerve head drusen were

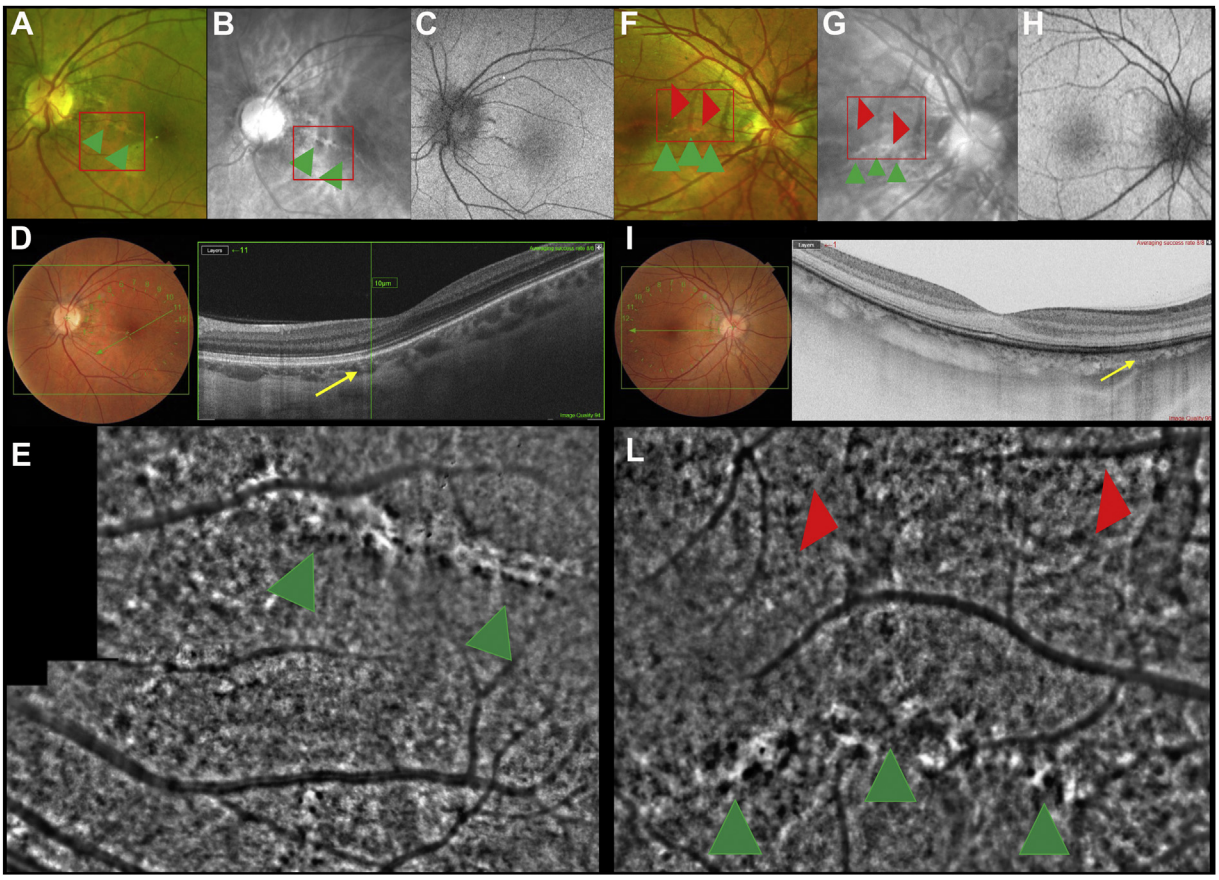

FIGURE 3. (A) CFP, (B) IR imaging, (C) FAF, (D) OCT, and (E) AO of the left eye of patient P6; (E) CFP, (F) IR imaging, (G) FAF, (H) OCT, and (I) AO of the right eye of patient P7. The red rectangle shows the AO image location. The multimodal imaging approach shows the clinical finding of Type 3 angioid streaks (hypopigmented type): the streaks appear whitish and hypopigmented at CFP (A, F) and hyper-reflective at IR imaging (B, G). OCT examination shows a thinning of the retinal pigment epithelium–Bruch membrane complex with the hyper-transmission phenomenon (yellow arrows) (D, I). AO examination (E, L) displays Type 3 angioid streaks (green arrowheads) as a diffused hyper-reflectivity due to the presence of hyper-reflective alterations detectable on and along these streaks. On the streaks, dark spots are also discernable, particularly evident at the boundaries. In patient P7, Type 2 angioid streaks are also visible (red arrowheads). AO = adaptive optics, CFP = color fundus photograph, FAF = fundus autofluorescence, IR = infrared, OCT = optical coherence tomography.

present in 2 eyes of 2 patients and appeared as dots of increased autofluorescence on FAF imaging.

In our series, peripheral comet lesions (CLs) were detectable in 10 eyes of 10 patients while peripapillary comet lesions (PCLs) were visible in 4 eyes of 4 patients. Both the CLs and PCLs appeared as whitish dot-like lesions on a gray background at the IR imaging and as small, hyperautofluorescent dots at the FAF examination; at OCT examinations, they appeared as ovoidal cavities of variable size with hyper-reflective borders at the level of the outer retinal layers.

Pattern dystrophy-like changes were identified in 3 eyes of 3 patients: all eyes were characterized as the "fundus pulverulentus" type.[11] At the funduscopic examination, pigment accumulations were detected at the posterior pole, which corresponded to hyper-reflective intraretinal lesions at the OCT examination. FAF imaging showed hyper- and hypo-autofluorescent lesions at the macula.

• **ADAPTIVE OPTICS IMAGING:** AO imaging was available for all eyes included in the study (21/21). Using AO imaging, we identified 3 different types of AS:

- Type 1 AS was visible in 8 eyes (8/21; 38.1%) of 8 patients, and it appeared as a well-defined jagged hyporeflective fissure more or less continuous. Hyperreflective changes could be detectable at the boundary of these streaks. The cone mosaic appeared not well-defined on the streaks, compared to the neighboring areas (Figures 1 and 2).
- Type 2 AS was identifiable in 12 eyes (12/21; 57.1%) of 8 patients and appeared as a hyporeflective band

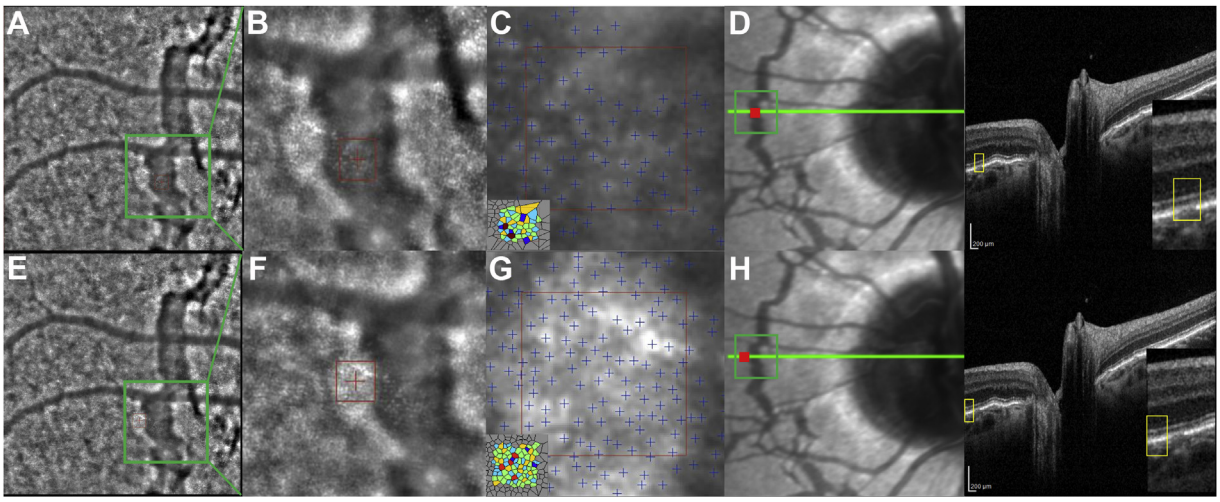

FIGURE 4. (A, E) AO imaging shows the appearance of the peripapillary Type 2 AS (band type) in the OD of patient P10. (B, F) Magnified AO images of the regions in the green square. Red squares represent the regions of interest (ROIs) where cones are measured; we considered the cone mosaic within the angioid streak in image B and the cone mosaic in the adjacent area (outside the angioid streak) in image F. (C, G) Results of cone counting on the AO high-resolution retinal imaging inside the AS (cone density: 12,344 cones/mm^2) (C), and in its absolute vicinity (cone density: 20,748 cones/mm^2) (G); the corresponding cone densities were represented on colored scale (bottom left). The custom software package (AO Detect Mosaic V.0.1) automatically detects the cone mosaic and the position of the photoreceptors. (D, H) Infrared images and horizontal SD-OCT scans passing through the ROI region (magnified in the bottom right box) showing a normal reflectivity of the external limiting membrane (ELM) and the ellipsoid zone (EZ) inside (D), and outside the AS (H) (yellow rectangle). The retinal pigment epithelium–Bruch membrane complex appears interrupted within the AS (D) and preserved along the boundary of the AS (H) (yellow rectangle). AO = adaptive optics, AS = angioid streaks, SD-OCT = spectral domain optical coherence tomography.

larger than Type 1. The central part showed a different reflectivity compared with the boundaries, which were more hyporeflective (dark). Hyper-reflective changes were evident at the outer boundaries of the streaks. Even in this case, the cone mosaic appeared not well-defined on the streaks compared to the neighboring areas (Figures 1-4).

- Type 3 AS was detectable in 3 eyes (3/21; 14.3%) of 3 patients and appeared as small, short, ill-defined streaks. It showed a diffused hyper-reflectivity owing to the presence of hyper-reflective alterations detectable on and along these streaks (Figure 3). On the streak, dark spots were also discernable, particularly evident at the boundaries. The cone mosaic also appeared less discernable on the streaks.

The AO imaging features have been summarized in Table 1.

Three eyes of 2 patients (P4, P10) presented both Type 1 and Type 2 AS, whereas 2 eyes of 2 patients (P6 and P7) presented both Type 2 and Type 3 AS. In both eyes of 1 patient (Patient P13), we did not detect AS using conventional and AO imaging, or even IR imaging. Cracked eggshell lesions appeared as Type 1 AS using AO imaging.

We also quantitatively evaluated the cone photoreceptors within the streaks and in the neighboring areas. In all eyes, the cone mosaic appeared reduced inside the streaks compared to the adjacent areas (13,532.8 ± 1,366.5 cones/mm^2 vs 16,817.1 ± 1,263.0 cones/mm^2) (Figure 4).

Using AO imaging, we were able to identify the comet lesions as hyper-reflective lesions of variable size surrounded by a hyporeflective border resembling a "dark halo." In 4 eyes of 4 patients we studied the PCL, whereas in 1 eye of 1 patient we evaluated a small comet lesion located at the posterior pole (Figure 5). The PCL appeared single and sometimes grouped in clusters. The cone mosaic appeared to be not well-defined on the PCL compared to the surrounding retina; more specifically, when the photoreceptors were detectable, they were characterized by an intense hyper-reflectivity.

In 2 eyes of 2 patients, we were able to identify the pigment accumulation (pattern dystrophy-like changes) as round hyporeflective abnormalities of the same size and morphology as the corresponding funduscopic lesions.

• **MULTIMODAL IMAGING CORRELATION OF THE AS:** We correlated the funduscopic, IR, and FAF imaging features with the AO findings. Regarding the angioid streaks, Type 1 appeared as a small reddish-brown or gray alteration at the funduscopic examination (and at color fundus imaging), a hyporeflective more-or-less continuous fissure at IR imaging, and as a hypo-autofluorescent abnormality at FAF imaging; we classified Type 1 as "crack type." Type 2

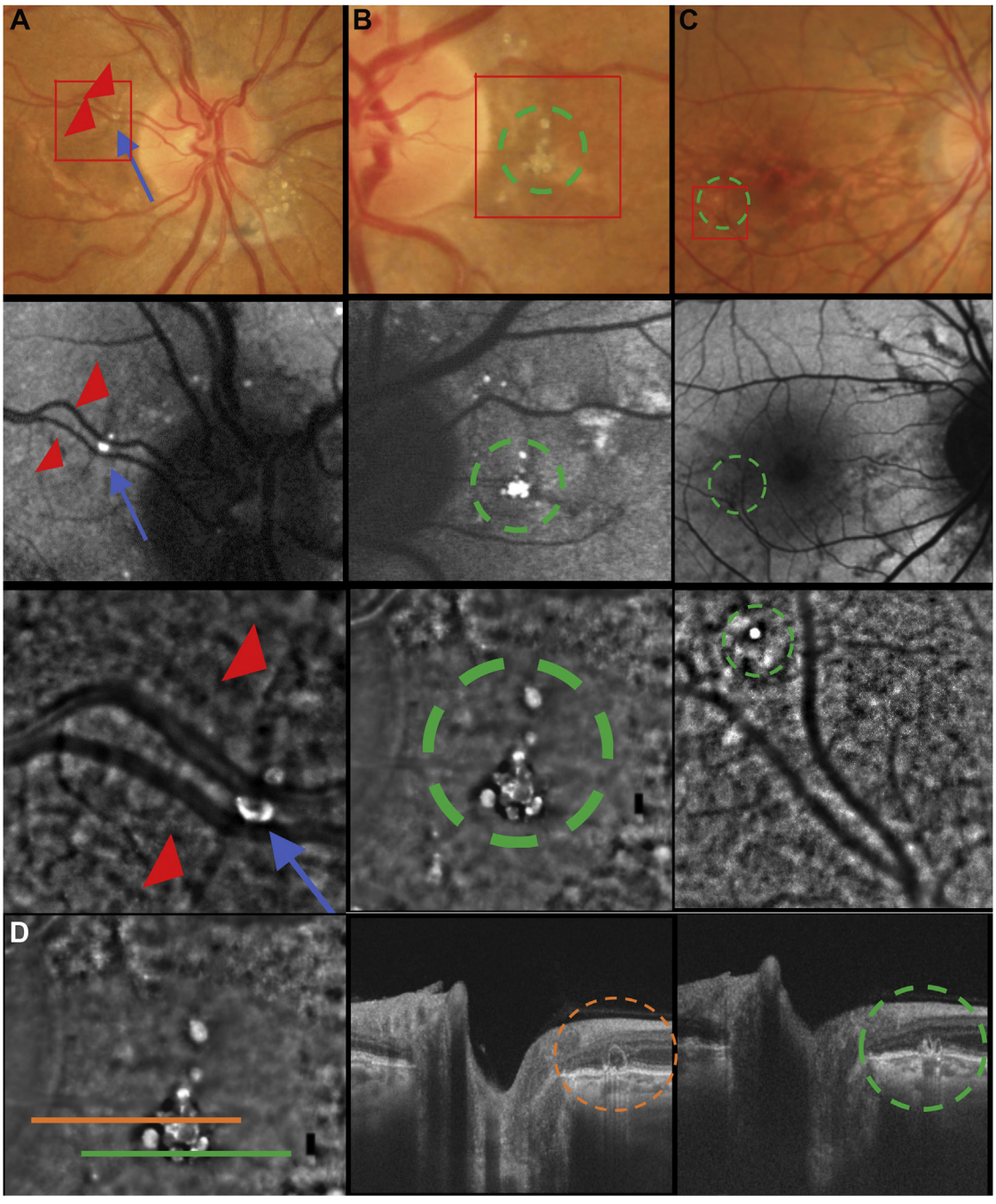

FIGURE 5. CFP, FAF, and AO of the (A) right and (B) left eyes of patient P16; (C) CFP, FAF, and AO of the right eye of patient P5. The red rectangle showing the AO image location. The images show the peripapillary comet lesions (A, blue arrows; B, green circle) and a small comet lesion at the posterior pole (C) (green circle). A small angioid streak (band type) is detectable in the right eye of patient P16 (A) (red arrowheads). Comet lesions are shown as hyper-reflective round lesions with a "dark halo" using AO. (D) AO image and OCT scans of the comet lesions of the left eye of patient P16: at the structural OCT, comet lesions appear as ovoid hypo-reflective lesions with hyper-reflective borders (orange and green circle). AO = adaptive optics, CFP = color fundus photograph, FAF = fundus autofluorescence, IR = infrared, OCT = optical coherence tomography.

appeared as a large reddish-brown or gray alteration at funduscopic imaging, a more-or-less large hyporeflective continuous band at IR imaging, and as a hypo-autofluorescent lesion at FAF imaging; we classified Type 2 as "band type." The Type 1 and Type 2 streaks were interconnected, and the main difference was the size of the streak. On OCT imaging, we detected the undulation and the interruption (of variable size) of the retinal

pigment epithelium–Bruch membrane complex in correspondence with the streak. The width of the AS on IR reflectance imaging corresponded to both the width of AS detectable on AO imaging and the Bruch membrane–retinal pigment epithelium complex interruption revealed on OCT.

Finally, the last type of angioid streak (Type 3) was completely different from the other 2. In fact, except for the hypo-autofluorescent features (which were similar to the others'), the streak appeared whitish and hypopigmented at funduscopic examination (and at color fundus photography) and hyper-reflective at IR imaging. At OCT examination, we were not able to identify the retinal pigment epithelium–Bruch membrane interruption but only a thinning of the retinal pigment epithelium–Bruch membrane complex with the hypertransmission phenomenon (Figure 3). There was a correspondence between the size and morphology of this AS type at fundus examination and using IR and AO imaging; however, the correspondence was less clear with OCT abnormalities owing to the absence of retinal pigment epithelium–Bruch membrane defects/interruption; we classified Type 3 as "hypopigmented type."

DISCUSSION

IN OUR SERIES, WE HAVE EVALUATED THE CLINICAL FINDings of PXE-related retinopathy using standard retinal and AO imaging modalities. As of this writing, only 2 articles have reported the retinal findings in PXE patients using AO imaging[16,17] and both papers described PXE-related features only in 1 patient. More specifically, Sampson and associates[17] described the angioid streaks in a 42-year-old woman as irregular linear hyporeflective lesions, whereas Onishi and associates[16] only examined the appearance of peau d'orange in a 41-year-old man.

Angioid streaks are irregular, linear, cracklike dehiscences of a calcified and brittle Bruch membrane, typically emerging as dark reddish-brown bands, with borders of variable width.[34–36] AS are most prominent at the posterior pole where they surround and radiate the optic disc and typically taper and fade toward the equator of the eye, often dividing into tiny branches; they could be attributed to mechanical stress exerted by the extraocular muscles on a fragile, and less flexible, posterior pole.[36,37] Infrared and red-free retinography, fundus autofluorescence, OCT, fluorescein angiography (FA), and indocyanine green angiography are the fundus imaging techniques useful to diagnose, evaluate, and monitor angioid streaks.[34–38]

To the authors' knowledge, this article is the first to analyze the appearance of AS and comet lesions in many PXE patients, using a multimodal imaging approach including adaptive optics.

Using a multimodal imaging approach, we identified 3 types of angioid streaks, which we have called crack, band, and hypopigmented. The first 2 types (crack and band) showed several analogies; in fact, they presented the same funduscopic features, already described in literature, using different imaging techniques (IR, FAF, OCT).[34–37] Using AO, the crack type appeared as a marked hyporeflective jagged line and the band type as a large hyporeflective streak (as a band) with dark hyporeflectivity only at the inner boundaries of the streak. Furthermore, AO better showed that these 2 types of AS were often interconnected. The principal difference between the crack and band types was the size of the AS; in fact, OCT examination better displayed the different Bruch membrane size defects. On the other hand, the third type of streak (hypopigmented type) was different from the previous 2; in our series, we were able to identify it only in 3 young patients (the elder 2 were 22 years old). At funduscopic examination, the hypopigmented type appeared as a hypopigmented/whitish linear abnormality unlike the reddish-brown appearance of the crack and band type; at IR imaging, it was hyper-reflective with indistinct boundaries compared with the well-defined hyporeflectivity of the other 2 streaks; at OCT scans, we did not identify retinal pigment epithelium–Bruch membrane breaks but only a slight thinning and a reduced reflectivity of the retinal pigment epithelium–Bruch membrane complex, which was confirmed by the presence of a hypertransmission phenomenon; similar funduscopic and OCT findings of the AS have already been described in rare cases.[37,39]

All these clinical findings were compatible with retinal pigment epithelium hypopigmentation and atrophic abnormalities,[37,40] and more specifically, the hypopigmented-type streaks were remarkably similar to the lacquer cracks described in pathologic myopia.[41,42] Patients P6 and P7 were myopic but patient P11 was emmetrope. Furthermore, AO examination helped to differentiate this streak through specific findings: a more-or-less evident diffused hyper-reflectivity with dark spots within and along the streak.

The hypopigmented type is characterized by retinal pigment epithelium–Bruch membrane complex hypopigmentation/thinning and atrophy rather than an evident interruption; so it may be possible that retinal pigment epithelial dysfunction (due to Bruch membrane abnormalities) is the major pathogenetic mechanism of these specific streaks, such as the lacquer cracks in myopia; in fact, we know that the retinal pigment epithelium on Bruch membrane breaks can be unaffected, even if it often appears altered.[35] Therefore, apart from the retinal pigment epithelium–Bruch membrane complex interruption due to calcification, which makes the Bruch membrane fragile followed by retinal pigment epithelial atrophic changes, it is possible to have linear atrophic retinal pigment epithelial abnormalities without retinal pigment epithelium–

Bruch membrane interruption in PXE. We cannot exclude that the crack-type and/or the band-type AS can develop from the hypopigmented type, or in their immediate proximity; in fact, retinal pigment epithelial alterations, mostly loss of pigment, have been observed adjacent to some AS[37]; however, very small streaks can be seen in pediatric patients without evidence of hypopigmentation.[18,43] For this reason, it is more likely that the retinal pigment epithelial hypopigmented abnormalities (with or without pigment clumping) are secondary to the development of crack-type or band-type AS.

Regarding the possible pathogenetic mechanisms of AS, it has been suggested that a thickening of Bruch membrane and/or a decrease of the pigment granules, pigment stripping, and mottling in the retinal pigment epithelium exist with or without concurrent disruption in the overlying layers of the retina and the underlying choriocapillaris,[44] so we assumed that 2 types of mechanisms are possible, both due to Bruch membrane alterations: a circumscribed retinal pigment epithelial hypopigmentation and atrophy (hypopigmented type, similar to the lacquer crack) and an abrupt interruption of the retinal pigment epithelium–Bruch membrane complex followed by atrophic changes.

We have described the comet lesion appearance in PXE using AO examination for the first time; AO imaging was able to identify very small lesions at the posterior pole, which appeared as hyper-reflective round lesions with a dark margin (dark halo), not easily detectable with other retinal imaging techniques.

Thanks to the AO examination, we were able to detect the presence of photoreceptors on some parts of the streaks, confirming the observations of other authors[17,37]; however, different reasons could be responsible for the lack of detection of photoreceptors in the remaining regions: the atrophic processes of the streak, and probably the reflectivity changes due to the variable depth of the streak compared to the adjacent retinal plane. Regarding the comet lesions, the photoreceptors were not usually identifiable throughout the entire lesion, and when they were detectable, they were characterized by an intense hyperreflectivity.

The limits of our study are the few eyes analyzed, even though we have to consider that PXE is a rare disease, and moreover a good fixation is required to perform the AO examination; for this reason, PXE patients with extensive atrophic abnormalities were excluded from the study; for the same reason, our results did not show advanced stages of the disease. Obviously, this is also a value, as we have reported the alterations in the early stages of the disease.

In conclusion, using adaptive optics imaging in PXE-related retinopathy, we were able to show the presence of photoreceptors within the angioid streaks, differentiate 3 types of angioid streaks based on size and reflective features, and identify the very small comet lesions not identifiable using other retinal imaging techniques.

ACKNOWLEDGEMENT

FUNDING/SUPPORT: THIS STUDY RECEIVED NO FUNDING. FINANCIAL DISCLOSURES: THE AUTHORS INDICATE NO FINANCIAL support or conflicts of interest. All authors attest that they meet the current ICMJE criteria for authorship.

Acknowledgments: Authors gratefully acknowledge the collaborative support of PXE Italia Onlus and the technical contribution of Sonia Costa.

REFERENCES

1. Li Q, Arányi T, Váradi A, Terry SF, Uitto J. Research progress in pseudoxanthoma elasticum and related ectopic mineralization disorders. *J Invest Dermatol* 2016;136(3):550–556.
2. Le Saux O, Urban Z, Tschuch C, et al. Mutations in a gene encoding an ABC transporter cause pseudoxanthoma elasticum. *Nat Genet* 2000;25(2):223–227.
3. Struk B, Cai L, Zäch S, et al. Mutations of the gene encoding the transmembrane transporter protein ABC-C6 cause pseudoxanthoma elasticum. *J Mol Med (Berl)* 2000;78(5):282–286.
4. Nitschke Y, Baujat G, Botschen U, et al. Generalized arterial calcification of infancy and pseudoxanthoma elasticum can be caused by mutations in either ENPP1 or ABCC6. *Am J Hum Genet* 2012;90(1):25–39.
5. Boraldi F, Lofaro FD, Costa S, Moscarelli P, Quaglino D. Rare co-occurrence of beta-thalassemia and pseudoxanthoma elasticum: novel biomolecular findings. *Front Med (Lausanne)* 2020;6:322.
6. Chen KJ. Angioid streaks and other retinopathy in pseudoxanthoma elasticum. *JAMA Ophthalmol* 2019;137(10):e193129.
7. Coleman K, Ross MH, Mc Cabe M, Coleman R, Mooney D. Disk drusen and angioid streaks in pseudoxanthoma elasticum. *Am J Ophthalmol* 1991;112(2):166–170.
8. Murro V, Mucciolo DP, Sodi A, et al. Peripapillary comet lesions and comet rain in PXE-related retinopathy. *Graefes Arch Clin Exp Ophthalmol* 2018;256(9):1605–1614.
9. Smith JL, Gass JD, Justice J Jr. Fluorescein fundus photography of angioid streaks. *Br J Ophthalmol* 1964;48(10):517–521.
10. Spaide RF. Peau d'orange and angioid streaks: manifestations of Bruch membrane pathology. *Retina* 2015;35(3):392–397.
11. Agarwal A, Patel P, Adkins T, Gass JD. Spectrum of pattern dystrophy in pseudoxanthoma elasticum. *Arch Ophthalmol* 2005;123(7):923–928.

12. Battaglia Parodi M, Romano F, Marchese A, et al. Anti-VEGF treatment for choroidal neovascularization complicating pattern dystrophy-like deposit associated with pseudoxanthoma elasticum. *Graefes Arch Clin Exp Ophthalmol* 2019;257(2):273–278.
13. Gliem M, Fimmers R, Müller PL, et al. Choroidal changes associated with Bruch membrane pathology in pseudoxanthoma elasticum. *Am J Ophthalmol* 2014;158(1):198–207.e3.
14. Murro V, Mucciolo DP, Giorgio D, et al. Pattern dystrophy-like changes and coquille d'oeuf atrophy in elderly patients affected by pseudoxanthoma elasticum. *Graefes Arch Clin Exp Ophthalmol* 2020;258(9):1881–1892.
15. Liang J, Williams DR, Miller DT. Supernormal vision and high-resolution retinal imaging through adaptive optics. *J Opt Soc Am A Opt Image Sci Vis* 1997;14(11):2884–2892.
16. Onishi AC, Nesper PL, Fawzi AA. Adaptive optics scanning laser ophthalmoscopy and multimodal imaging of peau d'orange in pseudoxanthoma elasticum. *Ophthalmic Surg Lasers Imaging Retina* 2017;48(5):436–440.
17. Sampson DM, Alonso-Caneiro D, Chew AL, et al. Enhanced visualization of subtle outer retinal pathology by en face optical coherence tomography and correlation with multi-modal imaging. *PLoS One* 2016;11(12):e0168275.
18. Murro V, Mucciolo DP, Giorgio D, et al. Coquille d'oeuf in young patients affected with pseudoxanthoma elasticum. *Ophthalmic Genet* 2019;40(3):242–246.
19. Viard C, Nakashima K, Lamory B, Paques M, Levecq X, Chateau N. Imaging microscopic structures in pathological retina using a flood-illumination adaptive optics retinal camera. *Ophthalm Technol* 2011;21:7885.
20. Muthiah MN, Gias C, Chen FK, et al. Cone photoreceptor definition on adaptive optics retinal imaging. *Br J Ophthalmol* 2014;98(8):1073–1079.
21. Götting C, Schulz V, Hendig D, et al. Assessment of a rapid-cycle PCR assay for the identification of the recurrent c.3421C>T mutation in the ABCC6 gene in pseudoxanthoma elasticum patients. *Lab Invest* 2004;84(1):122–130.
22. Chassaing N, Martin L, Mazereeuw J, et al. Novel ABCC6 mutations in pseudoxanthoma elasticum. *J Invest Dermatol* 2004;122(3):608–613.
23. Costrop LM, Vanakker OO, Van Laer L, et al. Novel deletions causing pseudoxanthoma elasticum underscore the genomic instability of the ABCC6 region. *J Hum Genet* 2010;55(2):112–117.
24. Pulkkinen L, Nakano A, Ringpfeil F, Uitto J. Identification of ABCC6 pseudogenes on human chromosome 16p: implications for mutation detection in pseudoxanthoma elasticum. *Hum Genet* 2001;109(3):356–365.
25. Boraldi F, Costa S, Rabacchi C, Ciani M, Vanakker O, Quaglino D. Can APOE and MTHFR polymorphisms have an influence on the severity of cardiovascular manifestations in Italian Pseudoxanthoma elasticum affected patients? *Mol Genet Metab Rep* 2014;1:477–482.
26. Noji Y, Inazu A, Higashikata T, et al. Identification of two novel missense mutations (p.R1221C and p.R1357W) in the ABCC6 (MRP6) gene in a Japanese patient with pseudoxanthoma elasticum (PXE). *Intern Med* 2004;43(12):1171–1176.
27. Pfendner EG, Vanakker OM, Terry SF, et al. Mutation detection in the ABCC6 gene and genotype-phenotype analysis in a large international case series affected by pseudoxanthoma elasticum. *J Med Genet* 2007;44(10):621–628.
28. Le Saux O, Beck K, Sachsinger C, et al. A spectrum of ABCC6 mutations is responsible for pseudoxanthoma elasticum. *Am J Hum Genet* 2001;69(4):749–764 [erratum in Am J Hum Genet 2001 Dec;69(6):1413] [erratum in Am J Hum Genet 2002 Aug;71(2):448].
29. Ringpfeil F, Lebwohl MG, Christiano AM, Uitto J. Pseudoxanthoma elasticum: mutations in the MRP6 gene encoding a transmembrane ATP-binding cassette (ABC) transporter. *Proc Natl Acad Sci U S A* 2000;97(11):6001–6006.
30. Gheduzzi D, Guidetti R, Anzivino C, et al. ABCC6 mutations in Italian families affected by pseudoxanthoma elasticum (PXE). *Hum Mutat* 2004;24(5):438–439.
31. Uitto J, Pulkkinen L, Ringpfeil F. Molecular genetics of pseudoxanthoma elasticum: a metabolic disorder at the environment-genome interface? *Trends Mol Med* 2001;7(1):13–17.
32. Meloni I, Rubegni P, De Aloe G, et al. Pseudoxanthoma elasticum: point mutations in the ABCC6 gene and a large deletion including also ABCC1 and MYH11. *Hum Mutat* 2001;18(1):85.
33. Guerra D, Roggiani J, Panico F, et al. ABCC6 mutations in Italian PXE patients; an update describing 22 novel mutations. *Connect Tissue Res* 2009;50:80–81.
34. Finger RP, Charbel Issa P, Ladewig M, Götting C, Holz FG, Scholl HP. Fundus autofluorescence in pseudoxanthoma elasticum. *Retina* 2009;29(10):1496–1505.
35. Charbel Issa P, Finger RP, Holz FG, Scholl HP. Multimodal imaging including spectral domain OCT and confocal near infrared reflectance for characterization of outer retinal pathology in pseudoxanthoma elasticum. *Invest Ophthalmol Vis Sci* 2009;50(12):5913–5918.
36. Chatziralli I, Saitakis G, Dimitriou E, et al. Angioid streaks: a comprehensive review from pathophysiology to treatment. *Retina* 2019;39(1):1–11.
37. De Zaeytijd J, Vanakker OM, Coucke PJ, De Paepe A, De Laey JJ, Leroy BP. Added value of infrared, red-free and autofluorescence fundus imaging in pseudoxanthoma elasticum. *Br J Ophthalmol* 2010;94(4):479–486.
38. Ellabban AA, Hangai M, Yamashiro K, Nakagawa S, Tsujikawa A, Yoshimura N. Tomographic fundus features in pseudoxanthoma elasticum: comparison with neovascular age-related macular degeneration in Japanese patients. *Eye (Lond)* 2012;26(8):1086–1094.
39. Ari Yaylali S, Akcakaya AA, Erbil HH, Salar S, Karakurt Y. Optical coherence tomography findings in pseudoxanthoma elasticum. *Eur J Ophthalmol* 2010;20(2):397–401.
40. Pfau M, Goerdt L, Schmitz-Valckenberg S, et al. Green-light autofluorescence versus combined blue-light autofluorescence and near-infrared reflectance imaging in geographic atrophy secondary to age-related macular degeneration. *Invest Ophthalmol Vis Sci* 2017;58(6):BIO121–BIO130 [erratum in: Invest Ophthalmol Vis Sci 2018;59(2):674].
41. Liu CF, Liu L, Lai CC, et al. Multimodal imaging including spectral-domain optical coherence tomography and confocal near-infrared reflectance for characterization of lacquer

cracks in highly myopic eyes. *Eye (Lond)* 2014;28(12):1437–1445.
42. Shinohara K, Moriyama M, Shimada N, Tanaka Y, Ohno-Matsui K. Myopic stretch lines: linear lesions in fundus of eyes with pathologic myopia that differ from lacquer cracks. *Retina* 2014;34(3):461–469.
43. Georgalas I, Kymionis G, Papakonstantinou D, Paraskevopoulos T. Angioid streaks in the fundus of a 13-year-old girl. *J Pediatr* 2016;179:269–269.e1.
44. Dreyer R, Green WR. The pathology of angioid streaks: a study of twenty-one cases. *Trans Pa Acad Ophthalmol Otolaryngol* 1978;31(2):158–167.